Environ. Sci. Technol. **2003**, *37,* 409−417

Sorption Hysteresis of Benzene in Charcoal Particles

WASHINGTON J. BRAIDA,[†,‡] JOSEPH J. PIGNATELLO,*[,†] YUEFENG LU,[†] PETER I. RAVIKOVITCH,[§] ALEXANDER V. NEIMARK,[§] AND BAOSHAN XING[||]

Department of Soil and Water, The Connecticut Agricultural Experiment Station, P.O. Box 1106, New Haven, Connecticut 06504-1106, TRI/Princeton, Princeton, New Jersey 08542, and Department of Plant and Soil Science, University of Massachusetts, Amherst, Massachusetts 01003

Charcoal is found in water, soil, and sediment where it may act as a sorbent of organic pollutants. The sorption of organic compounds to natural solids often shows hysteresis. The purpose of this study was to determine the source of pronounced hysteresis that we found in the sorption of a hydrophobic compound (benzene) in water to a maple-wood charcoal prepared by oxygen-limited pyrolysis at 673 K. Gas adsorption (N_2, Ar, CO_2), ^{13}C NMR, and FTIR show the charcoal to be a microporous solid composed primarily of elemental (aromatic) C and secondarily of carboxyl and phenolic C. Nonlocal density functional theory (N_2, Ar) and Monte Carlo (CO_2) calculations reveal a porosity of 0.15 cm^3/g, specific surface area of 400 m^2/g, and appreciable porosity in ultramicropores <10 Å. Benzene sorption−desorption conditions were chosen to eliminate artificial causes of hysteresis (rate-limiting diffusion, degradation, colloids effect). Charcoal sorbed up to its own weight of benzene at ∼69% of benzene water solubility. Sorption was highly irreversible over most of the range tested (10^{-4}−10^3 μg/mL). A dimensionless irreversibility index (I_i) ($0 \leq I_i \leq 1$) based on local slopes of adsorption and desorption branches was evaluated at numerous places along the isotherm. I_i decreases as C increases, from 0.9−1 at low concentration to ∼0 (∼fully reversible) at the highest concentrations. Using sedimentation and volumetric displacement measurements, benzene is observed to cause pronounced swelling (up to >2-fold) of the charcoal particles. It is proposed that hysteresis is due to pore deformation by the solute, which results in the pathway of sorption being different than the pathway of desorption and which leads to entrapment of some adsorbate as the polyaromatic scaffold collapses during desorption. It is suggested that intra-charcoal mass transport may be influenced by structural rearrangement of the solid, in addition to molecular diffusion.

Introduction

Black carbon (BC) refers to incompletely combusted residues of biomass and fossil fuel materials and includes charcoal and soot (*1*). BCs have been detected (or postulated to exist) in atmospheric aerosols (*2*), estuarine and deep-sea sediments (*3*, *4*), and soils (*5*), where their influence on transport and bioavailability of organic contaminants is thought to be of importance (*2*, *6*−*10*). The sorption of organic compounds to natural solids often shows hysteresis or irreversibility of the sorption−desorption cycle (*11*−*21*). Such compounds include pesticides (e.g., atrazine, lindane), chlorinated benzenes, and polycyclic aromatic hydrocarbons (PAHs) among others. Typically, the affinity of adsorbate for solid appears to be greater along the desorption branch than along the adsorption branch; in extreme cases, complete desorption cannot be achieved without vigorous intervention such as organic solvent extraction.

Two types of hysteresis are distinguished (*22*): *permanent or true hysteresis* caused by spontaneous mechanisms associated with pore filling and emptying and *artificial hysteresis* caused by an insufficient time allowed for diffusion equilibrium or some auxiliary process. The latter depends on conditions and can be eliminated, while the former is reproducible in repeated sorption−desorption cycles. Pollutant transport and bioavailability models generally rest on the assumption of sorption reversibility. Sorption coefficients used in such models are normally based on forward-constructed (adsorption) isotherms. If sorption is irreversible, these models will incorrectly predict the movement or biological fate of the chemical: contaminated materials may be less hazardous than expected; contaminant plumes in an aquifer may tail more extensively and require longer times to be flushed out; contaminated materials may prove resistant to biological, physical, or chemical treatment.

BCs have demonstrated high and nonlinear sorption of organic compounds (*6*, *10*). However, studies dealing with hysteresis in BCs are scant. Irreversible sorption implies that the microscopic pathways for adsorption and desorption are different. Hysteresis in mesoporous reference solids, which gives rise to a closed "hysteresis loop" at concentrations typically greater than 40% of the saturated vapor pressure, has been attributed to the attainment of metastable states associated with capillary liquid condensation (*23*). Hysteresis in microporous solids, on the other hand, is generally absent unless the pores are deformable by the adsorbate (*23*). Irreversible pore deformation is the assigned mechanism for hysteresis in the adsorption of alcohol vapors in the interlayers of dry clays (*24*, *25*) and in the adsorption of gases or hydrocarbon vapors in the nanovoids of glassy polymers (*26*, *27*).

BCs are composed of single and stacked polyaromatic sheets that are arranged in a highly disordered fashion (*1*, *28*−*30*). The sheets vary in size from a few to several tens of fused rings and may be functionalized along the edges. Chars may contain curved, fullerene-like structures that contribute to the disorder and prevent transformation to graphite at high temperature (*30*, *31*). The pore structure of BC is not well-known but has often been compared to that of activated carbons (*32*−*34* and references therein), which historically have been regarded as fixed-pore adsorbents (*35*). Deformation of activated carbon micropores is said to require breakage of covalent bonds (*36*).

The research herein investigated sorption−desorption hysteresis of benzene in a charcoal synthesized by pyrolysis of wood chips under oxygen-deficient conditions at 673 K. While this sample does not represent all charcoals in the environment, it does represent some. Adsorption−desorption isotherms were constructed spanning 7 orders of magnitude in concentration under conditions that rule out artificial

* Corresponding author e-mail: Joseph.Pignatello@po.state.ct.us. telephone: (203)974-8518; fax: (203)974-8502.

[†] The Connecticut Agricultural Experiment Station.

[‡] Present address: Center for Environmental Engineering, Stevens Institute of Technology, Hoboken, NJ 07030.

[§] TRI/Princeton.

[||] University of Massachusetts.

10.1021/es020660z CCC: $25.00
Published on Web 12/13/2002

causes of hysteresis. An index is proposed to quantify irreversibility. We find that this charcoal swells under the influence of benzene and propose a mechanism involving pore deformation to explain the high degree of sorption irreversibility.

Experimental Section

Materials. Charcoal was prepared by atmospheric pyrolysis according to a modification of the method of Glaser et al. (*37*). Maple-wood shavings were placed in a 15-cm watch-glass-covered crucible and heated at 673 K for 2 h. The yield of charcoal from four portions (14.5, 29.7, 31.1, and 34.9 g) was 24.7% ± 0.6%. The four batches were combined, pulverized gently in a mortar to pass through a sieve no. 100 (0.150 mm), and stored in a glass vial at room temperature. Elemental analysis (Galbraith Laboratories, Knoxville, TN) gave 71.97% C, 2.83% H, 0.51% N, and 2.03% ash. ^{14}C-Labeled benzene (58.2 mCi/mmol, 99+% radiolabel purity) and nonlabeled benzene (HPLC grade, 99.9+%) were from Sigma-Aldrich (St. Louis, MO).

Spectroscopic Analyses. The ^{13}C NMR spectrum of the charcoal was obtained by using CPMAS-TOSS techniques (cross-polarization magic-angle spinning with total sideband suppression). This method has proved valid for a wide range of organic samples from highly aromatic (coal humic acids) to highly aliphatic plant materials (*38*, *39*). The sample (~700 mg) was packed in a 7-mm-diameter zirconia rotor with a Kel-F cap and run at 75 MHz (^{13}C) in a Bruker DSX 300 MHz instrument. The spinning speed was 4.5 kHz. A ^{1}H 90° pulse was followed by a contact time (t_{cp}) of 1 ms, and then a TOSS sequence was used to remove sidebands (*38*, *39*). Contact time is sample-specific; preliminary tests determined 1 ms as optimal, as opposed to 0.5 ms used in our previous work (*38*). Line broadening of 30 Hz was used. The 90° pulse length was 3.4 μs, and the 180° pulse was 6.4 μs. The recycle delay was 1 s with the number of scans about 4096. There was no signal observed for the rotor and Kel-F cap (*38*), thus no background correction was necessary.

The diffuse reflectance FTIR spectrum (32 scans at 4 cm^{-1} resolution) was obtained on a Mattson Infinity Gold spectrophotometer using a SpectraTech Collector sampling cell. The charcoal concentration was 1.4% in KBr.

Pore Structure Characterization. Carbon dioxide (273 K), nitrogen (77 K), and argon (77 K) adsorption−desorption isotherms were measured volumetrically using an Autosorb-1C (Quantachrome Corp.) equipped with a Baratron 1 Torr pressure transducer. Temperature was controlled using a liquid nitrogen bath (N_2, Ar) or a homemade electric thermostat with an estimated accuracy of ±0.2 K (CO_2). Low-pressure adsorption data were corrected on the thermal transpiration effect according to standard procedures (Autosorb User Manual). For Ar at 77 K, the saturation pressure of the supercooled liquid Ar was used (P_0 = 230 Torr) (*40*). The saturation pressure of CO_2 at 273 K was taken to be 2.614 × 10^4 Torr. Separate experiments were done with samples vacuum-outgassed at 298, 373, and 573 K.

Pore size distribution, pore volume, and surface area were calculated from nonlocal density functional theory (NLDFT) and Monte Carlo (MC) molecular models, assuming slit-shaped pores with graphitic walls, as given in detail elsewhere (*41*, *42*). In this approach, the experimental isotherm is modeled as a collection of individual isotherms in pores of different sizes. N_2 and Ar were modeled as Lennard−Jones (LJ) fluids using NLDFT. CO_2 was modeled as a three-center LJ fluid with a quadrupole moment using the grand canonical MC simulations. Pore size distributions (PSD) were calculated by solving the generalized adsorption isotherm equation using regularization methods.

Benzene Adorption−Desorption. A known mass of charcoal (23 mg, oven-dry basis) was added to each of several 13-mL glass screw-cap tubes. Each tube was then filled to capacity with "simulant water," consisting of distilled−deionized water with 0.01 M $CaCl_2$ to simulate environmental water and 200 mg/L NaN_3 to inhibit degradation by incidental bacteria. The tubes were sealed with aluminum foil topped with a PTFE-lined cap and shaken for 17 days to allow the charcoal to hydrate. Duplicate tubes were then amended with 9.5 × 10^{-8} Ci ^{14}C-labeled benzene and unlabeled benzene in methanol. The mole fraction of methanol in the simulant water in all tubes was 0.002 and therefore not expected to affect benzene sorption. The tubes were rotated end-over-end 15 times per min for 32 days in the dark at 21 ± 1 °C. Shorter times were used in kinetic experiments. After centrifugation (750*g* for 30 min), 1 mL of the supernatant was assayed for radioactivity by liquid scintillation counting in 15 mL of Opti-Fluor (Packard Instrument Co.).

For desorption, 5.0 or 9.0 mL of supernatant was removed and immediately replaced. To ensure continuity of the liquid phase, the replacement fluid was benzene-free simulant water previously equilibrated at the same charcoal:solution ratio for 32 days. Volatilization losses during replacement were minimized by performing the operation quickly (<2 min per vial), inserting the syringe needle through the foil, and minimally disturbing the liquid. The tubes were resealed and mixed for an additional 32 days (fewer in kinetic runs). Sorbed benzene was calculated by the difference between mass added and mass in solution, subject to correction for bottle losses of benzene. Bottle losses were evaluated in tubes without charcoal and assumed linear with the equilibrium solute concentration. They varied between 1.8 and 8% of total benzene added—negligible as compared to the observed percentages of benzene remaining with the solid because of hysteresis.

Addressing Artifacts. Hysteresis can be due to experimental artifacts such as degradation, sorption to nonsettling colloids, or failure to reach equilibrium because of diffusion limitations. These artifacts have confounded many previous studies of hysteresis. We verified that none of these artifacts could explain the hysteresis here. Thus, we deal with a permanent or true hysteresis.

After the desorption step, some tubes were checked for benzene mass balance. The charcoal was extracted with acetonitrile at 70 °C (4 h). The benzene was then phase-transferred to dichloromethane (DCM) after dilution with water (acetonitrile:water:DCM, 10:20:5). DCM extracts with naphthalene as internal standard were analyzed by GC/FID (DB624 column; J&W Scientific, Folsom, CA). Benzene recovery based on GC quantitation was 99 ± 8%, indicating that biotic and abiotic transformations were negligible.

Sorption to colloids can lead to overestimation of the truly dissolved concentration. Artificial hysteresis can be observed if some colloids are removed when the supernatant is replaced in desorption steps. Although the replacement fluid here was simulant water that had previously been equilibrated at the same charcoal:solution ratio (thus any colloids removed would have been replenished), we nevertheless sought to rule out any interference because of possibly different colloid concentrations during adsorption and desorption steps. The colloid effect was evaluated by the solubility enhancement method. Open tubes of simulant water or supernatant of a centrifuged charcoal suspension were placed in a sealed Erlenmeyer flask containing benzene. After 7 days equilibration with the headspace at 21 °C, the tubes were sampled, extracted with DCM, and analyzed for benzene by GC. The solubility of benzene in the supernatant of a centrifuged charcoal suspension in simulant water (1678 ± 150 μg/mL; standard deviation of triplicates) was not statistically different (p = 0.05) from that in simulant water alone (1626 ± 92 μg/mL), showing that the colloid effect can be neglected. The

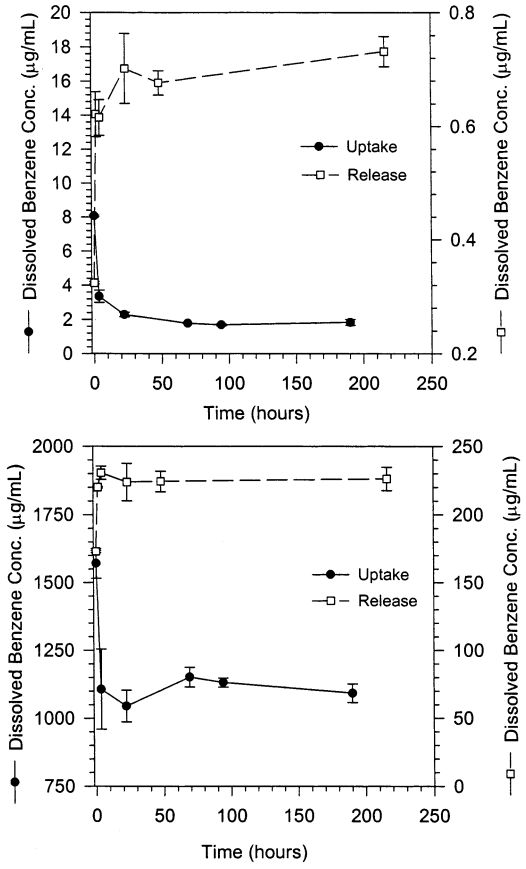

FIGURE 1. Change in the aqueous-phase benzene concentration over time for two different initial concentrations indicating apparent equilibrium after about 100 h for both adsorption and desorption to charcoal sample.

benzene solubility in pure water is reported to be 1780 μg/mL at 25 °C (*43*).

Finally, rate studies at two widely spaced initial concentrations indicated no significant changes in dissolved benzene concentration after ~100 h in both uptake and release experiments (Figure 1). This compares with an experimental equilibration period of 768 h for both adsorption and desorption branches of the isotherm.

Volumetric Swelling of Charcoal Particles. Two methods were employed: liquid displacement and sedimentation.

Liquid displacement followed a published technique for determining specific gravity (*44*). About 1 g of charcoal (the exact dry weight determined after completion of the experiment) was mixed with 5 mL of water in a round-bottom flask. The suspension was vacuum-degassed by three freeze−pump−thaw cycles to remove entrapped air bubbles in charcoal aggregates, then transferred to a calibrated 10-mL volumetric flask, and filled to the mark. After equilibration overnight at 24 ± 0.1 °C in an incubator, the volume was readjusted and the specific gravity of charcoal was determined accordingly to be 1.65. Swelling was conducted by incremental addition of liquid benzene to the suspension up to a total of 750 μL using a glass syringe. After each increment, the sample was rotated end-over-end in the incubator for 24−72 h. Volumetric changes were observed to be complete within 24 h. After allowing the particles to settle, the increase in volume was determined by withdrawing the extra supernatant with syringe to bring the level of fluid back to the mark. The withdrawn volume was determined volumetrically and confirmed by the difference in the weight of the flask before and after the withdrawal. Then the next increment of benzene was added, and the procedure was repeated. In no case was nonaqueous-phase benzene observed to be present after equilibrium.

The capacity of charcoal for water was determined by drying a known amount (~200 mg) of charcoal in an aluminum weigh boat at 105 °C overnight and then equilibrating the sample in an atmosphere saturated with water vapor in a closed vessel at 24 °C for 65 h. Water sorbed at equilibrium (~5 h) determined gravimetrically was 0.130 g of water/g of charcoal.

Sedimentation followed a modification of a published technique for measuring swelling of organic materials (*45*). A charcoal suspension in simulant water (1.25 g in 10 mL) was vacuum-degassed by three freeze−pump−thaw cycles. Aliquots of the suspension were loaded into tared, graduated Wintrobe tubes (3 mm i.d. × 115 mm long; catalog no. 36-402; Becton Dickinson, Franklin Lakes, NJ) to reach 80−90% capacity (~50 mg of charcoal). The tubes were centrifuged at 1800 rpm (750*g*) for 10 min, and the supernatant was removed. The tubes were exposed to radioactive antistatic electricity strips (Staticmaster Ionizing Units, SPI Supplies, West Chester, PA) and then filled to 80% capacity with simulant water or benzene-saturated simulant water and capped with plugs fashioned from Teflon rods. After being shaken to release air bubbles, the tubes were allowed to stand in a nearly horizontal position at 21 ± 0.2 °C. Three different sorbed concentrations were achieved by loading the Wintrobe tubes with benzene-saturated simulant water one, four, and seven times separated by 24 h. After a suitable time, the tubes were centrifuged at 750*g* for 10 min, and the heights of the charcoal columns were recorded. The centrifuge speed was the same, but the time was twice that of the original protocol (*45*); longer times had no further effect on charcoal column height. The volumetric swelling is defined as the ratio of the height of the charcoal column in a sedimentation tube containing benzene solution to the mean height of the charcoal column in tubes containing simulant water only. Since the amount of charcoal in each tube was slightly different, the column heights were all normalized to charcoal dry weight. At termination, an aliquot of the supernatant was extracted with DCM and analyzed for benzene by GC. The mass of charcoal was computed after drying the Wintrobe tubes for 6 h at 103 °C. The sorbed concentration was obtained from the experimental isotherm by interpolation.

Index of Irreversibility. The variation in irreversibility over the accessible isotherm can give insight into its causes. Several empirical models for calculating degree of sorption hysteresis in natural solids have been offered (*13*, *18*−*21*). However, those models are unsatisfactory here for a variety of reasons, particularly because they are not suitable for evaluating variation in hysteresis over the isotherm. Irreversibility cannot be defined thermodynamically, as has been done by Neimark (*46*, *47*), unless the hysteresis loop is closed.

Hysteresis is related to the tendency to desorb in response to dilution as compared with the hypothetical fully reversible and fully irreversible (zero desorption) cases. The tendency to desorb is given by the local rate of change (slope) of the isotherm at the point of interest. Refer to Figure 2. For an infinitesimal decrease in concentration starting from (C_i, q_i), the irreversibility index (I_i) can thus be defined as the difference in slopes of the adsorption and desorption isotherms divided by slope of the adsorption isotherm; i.e.

$$I_i = \frac{f'_a(C_i) - f'_d(C_i)}{f'_a(C_i)} \qquad (1)$$

where $f'_a(C_i)$ and $f'_d(C_i)$ are the first derivatives of the functions describing the adsorption and desorption branches, respectively, at C_i. Implicit in the denominator of eq 1 is the first derivative of the zero desorption branch, which is zero. Equation 1 is self-correcting for curvature of the whole

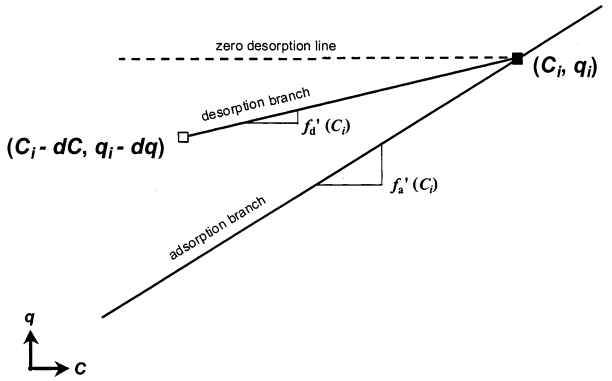

FIGURE 2. Schematic of the index of irreversibility in a segment of the isotherm covering an incremental change in concentration.

adsorption isotherm since it is normalized to $f_a'(C_i)$. For a single-point, infinitesimal desorption, eq 1 is equivalent to the ratio of mass that fails to desorb because of hysteresis to the mass expected to desorb if sorption were completely reversible.

For benzene in charcoal, the slope of each branch could only be estimated since the branches are not highly defined and fit to traditional isotherm functions was poor (see below). The slope of each desorption branch was obtained by fitting the available data (mean of several adsorption points plus one or two desorption points) to a linear equation. (Curvature should be minimal over the observed change in concentration, which was always <3-fold.) The adsorption branch was fit section-wise to a polynomial expression (third to sixth order, depending on the range: 0−0.01, 0.01−1.0, 0.75−25, 25−1000 μg/mL), and the slope at C_i was evaluated by differentiation. The curves near each C_i were tightly fit by the expression and very close to being linear.

Results

Adsorbent Characterization. Elemental analysis of the charcoal gives atomic ratios C/H equal to 2.13 and C/N equal to 165. The C/O ratio is ~4.2 if the balance of mass (~23%) is assumed to be O. [For comparison, a pine charcoal prepared in a similar way except at 600 K (*34*) gave a C mass content of 68.6%—vs 71.97% for our sample—and a C/N atomic ratio of 46.] The clear dominant peak at 130 ppm in the ^{13}C NMR spectrum (Figure 3) indicates that the charcoal is composed primarily of elemental (aromatic) C. There are no significant aliphatic resonances. Small peaks at 150 and 160−190 ppm reveal the presence of phenolic and carboxyl carbons. The FTIR spectrum (not shown), which probes a few tens of nanometers into the solid, gives strong peaks corresponding to carbonyl stretch (1610, 1700 cm^{-1}), C−O stretch (broad, centered at 1320 cm^{-1}), and hydrogen bonded -OH (broad, centered at ~3450 cm^{-1}). The presence of oxygenated functional groups indicated by the ^{13}C NMR and FTIR spectra is consistent with the high O content by elemental analysis. These groups are likely due to oxidation of carbons at the edges. The lack of aliphatic ^{13}C NMR resonances indicates the comparative absence of incompletely pyrolyzed lignocellulose structures.

The N_2 and Ar adsorption isotherms at 77 K on a sample vacuum-outgassed at 573 K (Figure 4) are classic type I (*23*), indicating microporous material with no significant mesoporosity. Despite long equilibration times (e.g., for Ar it took ca. 60 h to acquire the first three data and 70 more h for subsequent data), the isotherms are irreversible and exhibit a hysteresis loop, whose shape is not associated with capillary condensation in mesopores (*23*, *48*) but indicates that equilibrium was not fully achieved. Nonequilibrium may be due to severe diffusion limitation to passage through

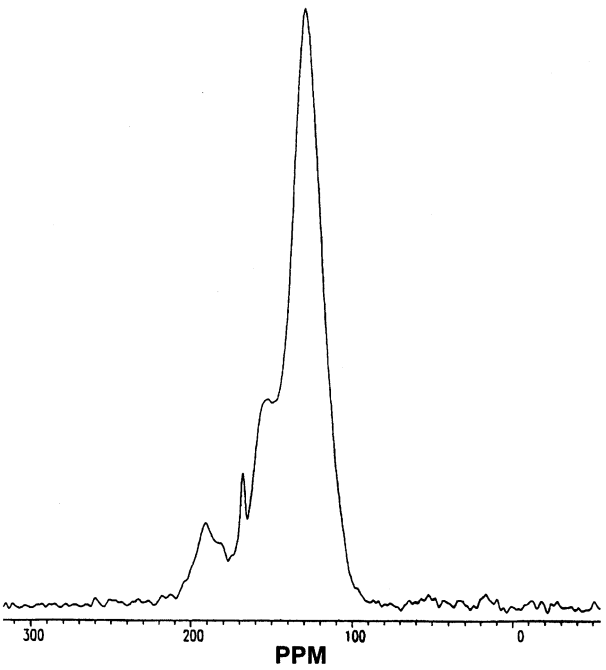

FIGURE 3. Solid-state ^{13}C NMR spectrum of charcoal sample.

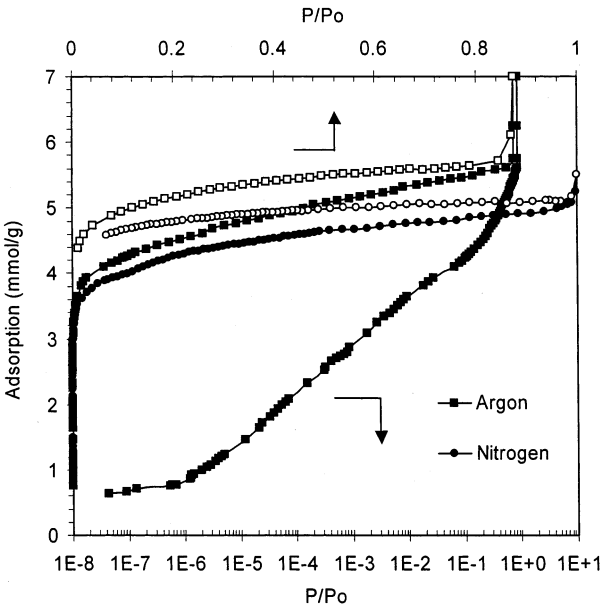

FIGURE 4. Nitrogen (circles) and argon (squares) adsorption isotherms at 77.4 K on charcoal sample vacuum outgassed at 573 K. Closed symbols, adsorption points; open symbols, desorption points. The argon isotherm is shown in both linear and logarithmic pressure scales. The N_2 isotherm has 150 data collected over 50 h. The Ar isotherm was constructed in two parts: the first has 3 data collected over 60 h; the second has 132 data collected over 70 h.

constricted pores at such a low temperature, or by structural rearrangement/relaxation of the adsorbent during sorption. A small plateau on the Ar isotherm at low relative pressures indicates very narrow micropores, whose equilibrium filling pressure is below the minimal measurable pressure. N_2 and Ar adsorption isotherms on a sample vacuum-outgassed at 373 K (not shown) were qualitatively similar to those for the sample outgassed at higher temperature but exhibited about half the sorption, indicating some residual amount of volatile substances blocking pores at the lower outgassing temperature. By contrast, CO_2 adsorption isotherms on charcoal

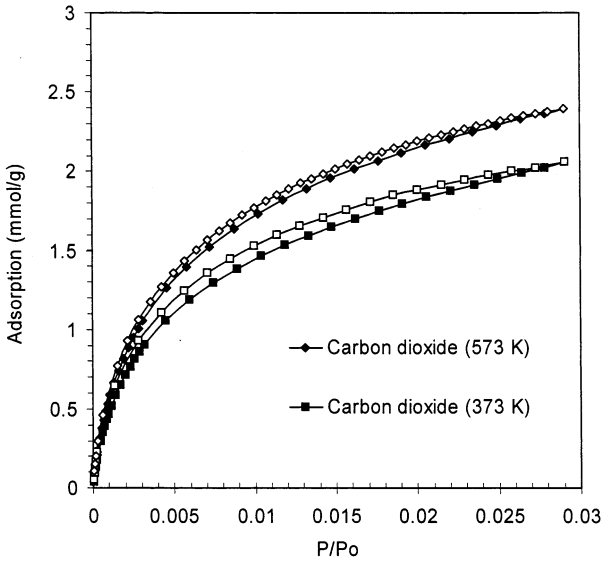

FIGURE 5. Carbon dioxide adsorption isotherms at 273 K on charcoal sample vacuum outgassed at 573 (diamonds) and 373 K (squares). Closed symbols, adsorption points; open symbols, desorption points. The 82 data were collected over 36 h.

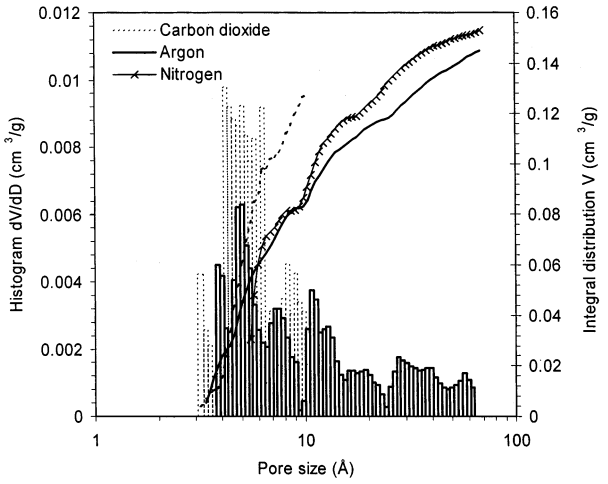

FIGURE 6. Pore volume distributions of charcoal sample (vacuum outgassed at 573 K) calculated from Ar, N_2, and CO_2 adsorption isotherms by means of the NLDFT (Ar, N_2) and MC models (for CO_2). For N_2, only the integral distribution is shown.

vacuum-outgassed at 373 and 573 K (Figure 5) differ by only 14% and give essentially the same pore size distribution. The isotherms exhibit very small hysteresis, which can thus be neglected. CO_2 adsorption at 273 K is known to be much less susceptible to diffusion limitations often encountered at cryogenic temperatures. The upper limit of pores probed by CO_2 at 273 K below 1 atm is ~10 Å (ultramicropores).

The pore size distributions (Figure 6) calculated from the adsorption branch using NLDFT model for Ar and N_2 and using MC model for CO_2 indicate that at least 50% porosity exists in pores <10 Å, with peak porosity occurring at ~4−6 Å. The pore size here is defined to the "edges" of the carbon atoms in the pore wall, taking 3.4 Å as the size of the carbon atom (*41*). The pore size distributions obtained from CO_2 and Ar are in good agreement; however, CO_2 gives ~60% higher volume of pores <10 Å because not all of these micropores are accessible to N_2 and Ar at 77 K. [It should be noted that activated carbon fibers, having most pores between ~4 and 10 Å, give very similar pore volume distributions for N_2, Ar and CO_2 (*41*).] The N_2 and Ar pore size distributions agree well and indicate that the charcoal is ca. 80% microporous (pores <20 Å). The total pore volume of charcoal outgassed at 573 K from N_2 and Ar measurements is ~0.15 cm^3/g; the total surface area (plot not shown) is ~400 m^2/g. The true numbers are likely to be greater, as not all of the porosity could be accessed at 77 K. For comparison, the BET surface area (*49*) based on N_2 is 340 m^2/g with nonphysical, strongly negative constant C. It should also be noted that the total pore volume of ~0.15 cm^3/g determined with N_2 and Ar agrees very well with the capacity of the charcoal for water (0.13 g of water/g; see below) assuming that the water density in pores is 1 g/cm^3.

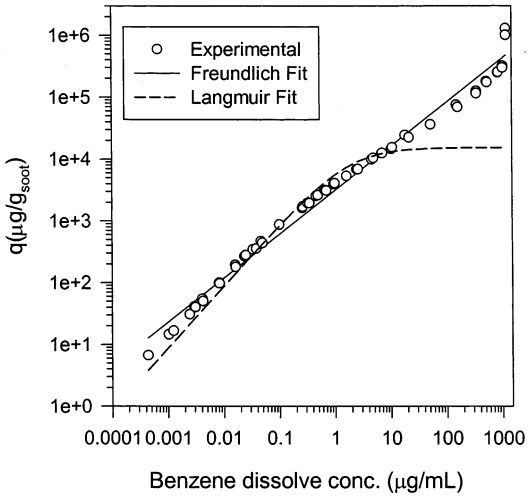

FIGURE 7. Adsorption isotherm of benzene in maple-wood charcoal on log scale. The Freundlich equation is $q = K_F C^n$, where q is the adsorbed concentration, C is the solute concentration, K_F is the Freundlich sorption coefficient, and n is the Freundlich exponent. The Langmuir equation is $q = QbC/(1 + bC)$, where Q is the capacity coefficient and b is the affinity coefficient.

Benzene Adsorption−Desorption Hysteresis. A 768-h (32-day) equilibration period was used to construct the adsorption and desorption branches of the isotherm—far longer than it took for the solution concentration to reach stasis (Figure 1). Figure 7 shows the adsorption isotherm on log-scale which spans 7 orders of magnitude in benzene concentration. Popular models such as Freundlich and Langmuir did not provide good fits. Figure 8 reproduces the adsorption isotherm on linear scale, zooming progressively from panel a to panel d. Note (panel a) the sharp rise in the isotherm beginning at about 1000 μg/mL or about 60% of benzene's water solubility. This rise was reproduced in an independent experiment. At about 1150 μg/mL (~69% of solubility), the charcoal is sorbing its own weight in benzene.

Figure 8 also includes the desorption branches coming off each adsorption equilibrium point. The desorption points correspond to 40% or 70% replacement of the liquid phase with clean simulant water. The isotherm shows pronounced hysteresis along almost the entire range of dissolved benzene concentration tested—from 1×10^{-4} μg/mL, which is close to the limit of quantification, to 1020 μg/mL, which is 61% of solubility. Above ~1050 μg/mL, hysteresis appears negligible.

Figure 9 shows the index of irreversibility (I_i) as a function of the log of dissolved benzene concentration. The index ranges from 0.9 to 1.0 at concentrations below $\sim 10^{-5}$ of solubility and then gradually decreases to ~0.6 by about half solubility. Above 1050 μg/mL, the index was disregarded because of the steepness and lack of definition in the adsorption branch, but I_i in that region appears from Figure 8 to be close to zero.

Sorbate-Induced Alteration of Charcoal Particles. Two different methods demonstrate that benzene causes swelling

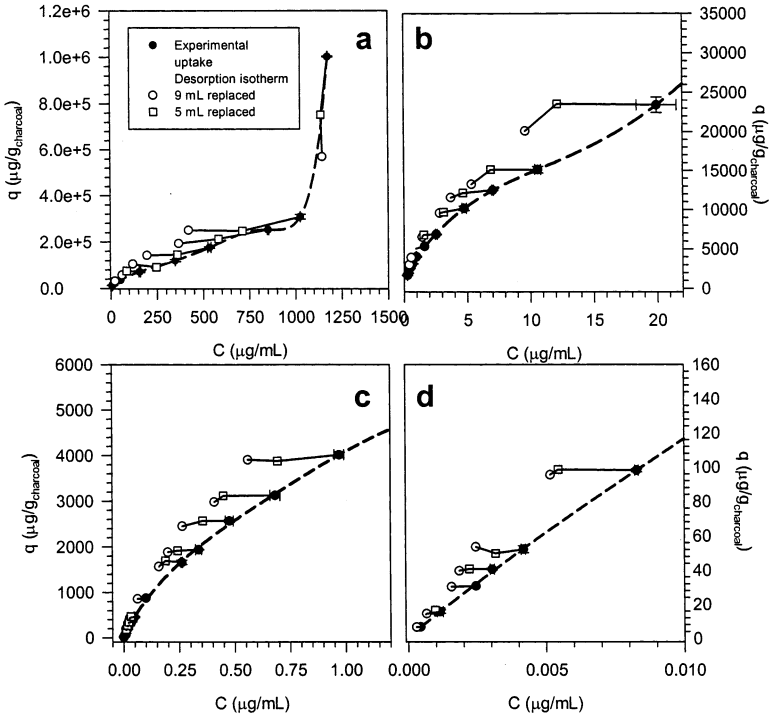

FIGURE 8. Sorption−desorption isotherms for benzene in charcoal sample on linear scale with zoom progressing from panel a to panel d. Lines are visual aids only.

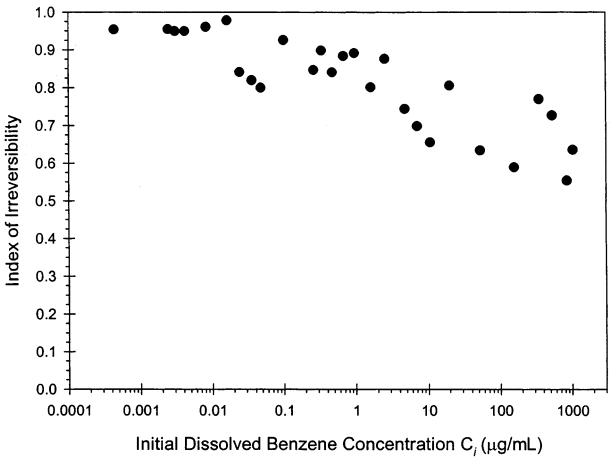

FIGURE 9. Index of irreversibility in charcoal sample assigned to points of origin (C_i) of the desorption branches along the benzene concentration axis in Figure 8. Uncertainty in I_i is estimated to be within 0.2.

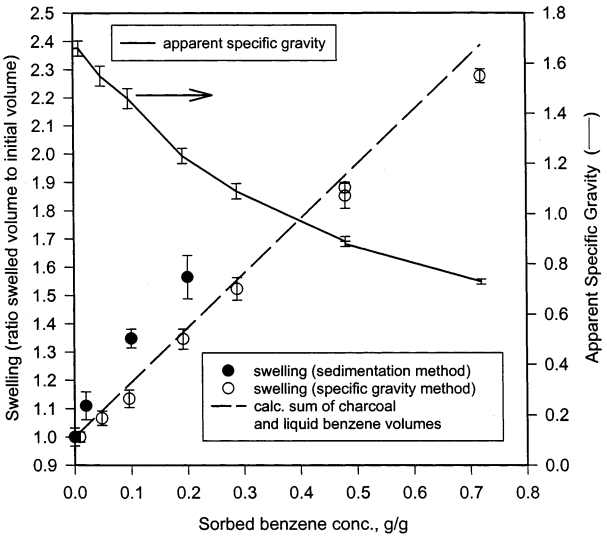

FIGURE 10. Volumetric swelling of charcoal sample by benzene using two different methods. Dashed line represents the sum of volumes of original charcoal and added pure liquid benzene (density 0.8765 g/cm^3 at 20 °C). Bars represent propagated sample standard deviation of 3−4 replicates (sedimentation data) or propagated estimated error of measurement (specific gravity data). Reproducibility of the specific gravity method was verified by adding 0.48 g of benzene/g in one portion rather than incrementally and obtaining the same result.

of the charcoal and, thus, deformation of the charcoal pore structure. Both methods are necessarily restricted to the high-concentration end of the benzene isotherm (2×10^4 μg/g) because of their low sensitivity.

The first is based on the method of specific gravity (*44*) and simply gives the displacement of aqueous fluid by charcoal or by charcoal sorbed with benzene. Figure 10 shows that sorption of benzene causes an increase in the volume occupied by the charcoal. There is also a corresponding decrease in the apparent specific gravity of the pure charcoal (not including adsorbate mass) from 1.65 for the original material to 0.73 for the sample exposed to the highest benzene concentration. The changes were complete within 24 h and reproducible (legend to Figure 10). The volumetric increases can be attributed to swelling. The swelling is slightly less than that calculated from the sum of the original charcoal and pure liquid benzene volumes (dashed line in Figure 10). Thus, at these (high) concentrations, benzene molecules swell the charcoal by an amount almost equal to their liquid volume. We reiterate that no nonaqueous-phase benzene was observed in the test vessel at equilibrium. The possibility that the volumetric changes are due merely to displacement of water by benzene in *fixed* pores can be ruled out because the capacity of the charcoal for water at 24 °C and 100% relative humidity is only 0.13 g of water/g, which places an upper limit on the ratio of "swelled" volume to initial volume of 1.21, a value that was clearly exceeded at benzene concentrations above ~0.1 g/g (Figure 10). Looked at another

way, the maximum observed swelling (2.3 at 0.72 g of benzene/g) corresponds to a water capacity of 1.39 g of water/g or 10.7 times more than measured. The validity of the fixed pore concept of charcoal—at least with respect to benzene—is weakened further by noting that, if it is assumed that the density of benzene condensed in pores approximates that of liquid benzene (0.8765 g/cm^3), the "porosity" of the charcoal reaches unity—i.e., the matrix occupies no volume at all!—at ~0.53 g of benzene/g, which is half or less of the charcoal's ultimate capacity for benzene.

The second method is a sedimentation technique (*45*) in which the height of a unit mass of charcoal in a column after centifugation is determined as a function of sorbed benzene concentration. Figure 10 indicates that benzene causes a volumetric change in the charcoal in relation to its concentration according to this method. Swelling is significant (at the 95% level) even at the lowest concentration tested, 0.02 g of benzene/g. Thus, sedimentation confirms the trends obtained by the specific gravity method. The greater swelling obtained by sedimentation could be due to buoyancy effects not overcome by centrifugation (*45*) as the particles become imbibed with benzene.

Discussion

Hysteresis of benzene in this sample of charcoal is not due to common artifacts like degradation, the colloids effect, or rate-limiting diffusion (see Experimental Section); it therefore represents spontaneous (irreversible) mechanisms associated with pore filling and emptying. Since pronounced irreversibility exists while benzene is filling micropores—even down to 10^{-7} times solubility—it cannot be attributed to capillary condensation phenomena that are characteristic of fixed mesopore systems (*23*). The most likely explanation for the hysteresis of benzene in this charcoal is irreversible pore deformation by the sorbate. This produces a situation in which adsorption and desorption occur to/from different microenvironments. The pore deformation hypothesis is supported by liquid displacement and sedimentation measurements that conclusively demonstrate swelling. Swelling means that the internal matrix expands in response to the presence of the adsorbate. A linkage between swelling and hysteresis in this material is rational given the behavior of microporous standards. Sorption hysteresis of polar compounds in dry smectite clays and nonpolar compounds in organo-substituted clays has been attributed to irreversible expansion of the interlayer (*24*). Hysteresis in glassy polymers has been attributed to irreversible deformation by the sorbate of internal nanopores inherent in such materials (*26, 27*). We have proposed the latter type of hysteresis in soil organic matter based on isotherms of trichloromethane and other compounds (*16, 17*).

The pore structure of BC particles is not well-understood and probably depends greatly on formation conditions. Gas adsorption shows the charcoal to have a heterogeneous micropore structure, including pores <4 Å in width. Transmission electron micrographs of an anthracene soot (*29*) clearly show the presence of open and closed micropores, most only 3−4 Å in width. In some diesel soots, the ratio of N_2 BET surface area to the calculated smooth-sphere external surface area based on electron microscopy was close to unity (*10, 28, 50*). This and the observation that diesel soot uptake of PAHs occurs within hours to days (*10*) led some authors to suggest that accessible soot micropores might extend only a short distance into the solid and that sorption occurs on the external skin of the particles (*10, 28*). Evidently, however, charcoal (this study; *51*) and perhaps diesel soots (*10*) (see below) can be swelled by the solute. Swelling may open up previously inaccessible pores. If this occurs, it could provide a basis for irreversible sorption. We propose the following mechanism for irreversible pore deformation.

SCHEME 1[a]

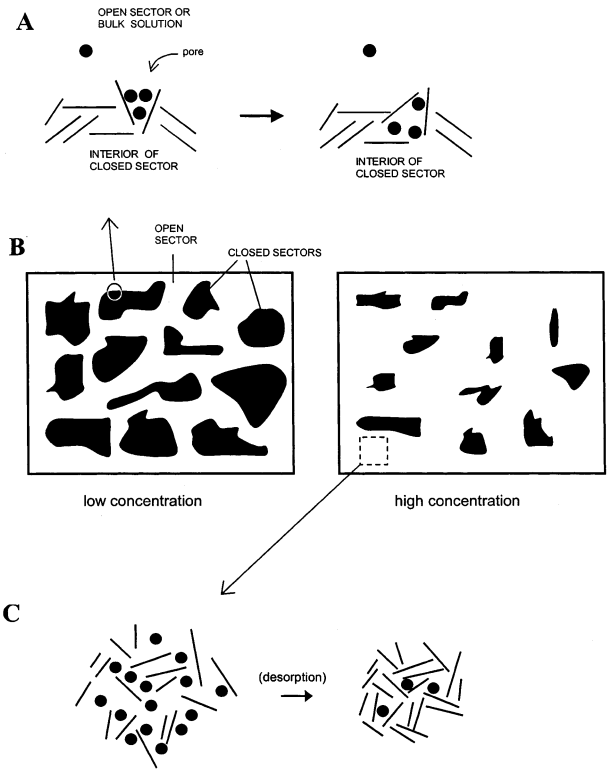

[a] Key: (Panel A) Leakage of adsorbate molecules into closed sectors of charcoal particle. (Panel B) Adsorbent volume of closed sectors (black areas) is reduced as external solute pressure increases. (Panel C) On desorption, some open sector reverts to closed sector, hindering release of molecules further in. Some adsorbate molecules are entrapped in the nascent closed sector

The original elementary charcoal particle may reasonably be considered to contain *open sectors* and *closed sectors* with respect to an adsorbate (Scheme 1B). Open sectors are understood to have pores that have a high degree of connectivity and that are in thermodynamic contact with bulk solution. Closed sectors are understood to have the opposite. As benzene enters the solid, it adsorbs in micropores in the open sectors. In response to the presence of the adsorbed benzene, some rearrangement of polyaromatic sheets making up the pore wall occurs, causing expansion of some of the pores. This behavior is expected because (a) pressure is exerted by the adsorbate on the pore walls and (b) sheets bounding the pore are held together in part by noncovalent weak forces. Expansion of the pores now opens up new pathways for benzene molecules to penetrate into previously closed sectors. In some instances (Scheme 1A), the "door shuts behind the adsorbate", trapping it in the closed sector until further rearrangement at some future time opens up a pathway for its escape. Closed sectors would then contain adsorbate that has leaked in but is unable to leak out on short time scales. Although swelling is confirmed only in the bulk sample at high concentrations, it is reasonable to expect it to occur at the local level at low concentrations because pore expansion is a function of *local* benzene concentration, which can be high in a narrow hydrophobic pore even at low solute concentration; thus, hysteresis is observed throughout the isotherm.

Matrix expansion also means that part of the work of adsorption is converted to entropy in the form of increased pore surface area. Expansion is not expected to be completely reversible because of the restricted mobility of the polyaromatic sheets. Hence, the adsorbate experiences a stronger net affinity for the adsorbent in the desorption direction than in the adsorption direction, giving rise to hysteresis.

Penetration of adsorbate causes softening of the matrix, as adsorbate−adsorbent interactions develop at the expense of adsorbent−adsorbent interactions. The degree of softening depends on the local adsorbate concentration, which, in turn, depends on external solute pressure. The effect of softening is to convert closed-sector volume to open-sector volume, effectively increasing the free diffusion space of the adsorbate. Thus, as external solute pressure increases, the adsorbent volume occupied by closed sectors is reduced (Scheme 1B). This accounts for the decline in the index of irreversibility as concentration increases (Figure 9). The closed sector volume may reach zero as the particles swell to twice or more their original size at very high concentrations (Figure 10); indeed, hysteresis practically disappears at the highest concentrations (Figure 8). Softening also depends on adsorbate structure. Benzene sorption is seen to be more hysteretic than CO_2 sorption. This is because benzene interacts more strongly with charcoal than CO_2 since it is larger, more polarizable, and undergoes stronger van der Waal interactions with polyaromatic sheets.

An additional effect of pore deformation is manifested during net desorption. As the external fluid concentration is suddenly reduced, the flux of adsorbate leaving the solid causes contraction of pores and thus reversion of open-sector to closed-sector volume. During this reversion, some benzene molecules may end up trapped in the nascent closed sector as the polyaromatic scaffold around them collapses (Scheme 1C).

Hysteresis, in summary, is a consequence of the following: (i) leakage of penetrant during net adsorption into closed sectors where it is no longer in thermodynamic contact with solute in bulk solution; (ii) irreversible pore expansion; and (iii) contraction of pores during net desorption and trapping of adsorbate within the collapsed structure. The foregoing mechanism implies that intra-grain transport is dependent on matrix rearrangement processes in addition to passive diffusion of the penetrant. Since it is the former that gives rise to irreversibility, it follows that reversibility would be achieved if uptake and release were to occur over an infinite number of steps over infinite time.

Support for a pore deformation mechanism in BC also exists in the recent literature. The possibility of pore dilation in carbonaceous adsorbents caused by the packing effects of adsorbate molecules has been discussed by Olivier (*52*). The water−diesel soot partition coefficient of naphthalene calculated by moments analysis of elution curves was greater on a soot column preconditioned with methanol (*10*), suggesting that methanol might have swelled the soot. While this manuscript was under revision, Jonker and Koelmans (*51*) reported that organic solvents differ in their ability to extract PAHs from soots and charcoals, leading them to postulate a swelling mechanism. Our study together with these (*10*, *51*, *52*) show that environmental BCs cannot be regarded as fixed-pore adsorbents inert to the adsorbate. Clearly, further studies on charcoals prepared from different materials and under different thermal conditions are justified to see if this generalization is true.

Our results are tentatively restricted to benzene and other molecules of similar size. Larger molecules such as PAHs may have smaller open sectors available to them initially. In the limit of increasing size, the open sector would be the external surface. It has been suggested that 2−4-ring PAHs sorb only on external surfaces of diesel particles (*10*), but the kinetic evidence for this is inferential and not rigorous. It is also possible that diesel soot is a more rigid material than the charcoal of our study. We speculate that larger molecules have the ability to swell BC (at least charcoal) but on longer time scales. With increasing penetrant size, dispersion interactions with the sorbent increase, facilitating pore deformation, but diffusion slows due to steric hindrance.

Acknowledgments

This work was supported by grants from the U.S. Environmental Protection Agency (R 82595-01-0) and the National Science Foundation (BES 0122761). The authors thank Jason White for discussion and comments on the manuscript.

Literature Cited

(1) Goldberg, E. D. *Black Carbon in the Environment*; John Wiley & Sons: New York, 1985.
(2) Lighty, J. S.; Veranth, J. M.; Sarofim, A. F. *J. Air Waste Manage. Assoc.* **2000**, *50*, 1565−1618.
(3) Maruya, K. A.; Risebrough, R. W.: Horne, A. J. *Environ. Sci. Technol.* **1996**, *30*, 2942−2947.
(4) Masiello, C. A.; Druffel, E. R. *Science* **1998**, *280*, 1911−1913.
(5) Skjemstad, J. O.; Taylor, J. A. *Commun. Soil Sci. Plant Anal.* **1999**, *30*, 2283−2298.
(6) Gustafsson, O.; Haghseta, F.; Chan, C.; Macfarlane, J.; Gschwend, P. M. *Environ. Sci. Technol.* **1997**, *31*, 203−209.
(7) McGroddy, S. E.; Farrington, J. W.; Gschwend, P. M. *Environ. Sci. Technol.* **1996**, *30*, 172−177.
(8) Broman, D.; Naf, C.; Wik, M.; Renberg, I. *Chemosphere* **1990**, *1−2*, 69−77.
(9) Karapanagioti, H. K.; Kleineidam, S.; Sabatini, D. A.; Grathwohl, P.; Ligouis, B. *Environ. Sci. Technol.* **2000**, *34*, 406−414.
(10) Bucheli, T. D.; Gustafsson, O. *Environ. Sci. Technol.* **2000**, *34*, 5144−5151.
(11) Miller, C. T.; Pedit, J. A. *Environ. Sci. Technol.* **1992**, *26*, 1417−1427.
(12) Kan, A. T.; Fu, G.; Tomson, M. B. *Environ. Sci. Technol.* **1994**, *28*, 859−862.
(13) Huang, W.; Weber, W. J., Jr. *Environ. Sci. Technol.* **1997**, *31*, 2562−2569.
(14) Kan, A. T.; Fu, G.; Hunter, M. A.; Tomson, M. B. *Environ. Sci. Technol.* **1997**, *31*, 2176−2186.
(15) Kan, A. T.; Fu, G.; Hunter, M.; Chen, W.; Ward, C. H.; Tomson, M. B. *Environ. Sci. Technol.* **1998**, *32*, 892−902.
(16) Xia, G.; Pignatello, J. J. *Environ. Sci. Technol.* **2001**, *35*, 84−94.
(17) Lu, Y.; Pignatello, J. J. *Environ. Sci. Technol.* **2002**, *36*, 4553−4561.
(18) Laird, D. A.; Yen, P. Y.; Koskinen, W. C.; Steinheimer, T. R.; Dowdy, R. H. *Environ. Sci. Technol.* **1994**, *28*, 1054−1061.
(19) Zhu, H.; Selim, H. M. *Soil Sci.* **2000**, *165* (8), 632−645.
(20) Ma, L.; Southwick, M.; Willis, G. H.; Selim, H. M. *Weed Sci.* **1993**, *41* (4), 627−633.
(21) Cox, L.; Koskinen, W. C.; Yen, P. Y. *J. Agric. Food Chem.* **1997**, *45*, 1468−1472.
(22) Everett, D. H. In *The Solid−Gas Interfac*e, Vol. 2; Flood, E. A., Ed.; Marcel Dekker: New York, 1967; Chapter 36.
(23) Rouquerol, F.; Rouquerol, J.; Sing, K. *Adsorption by Powders and Porous Material*; Academic Press: San Diego, 1999.
(24) Barrer, R. M. *Zeolites and Clay Minerals*; Academic Press: London, 1978.
(25) Tvardovski, A. V.; Fomkin, A. A.; Tarasevich, Yu. I.; Zhukova A. I. *J. Colloid Interface Sci.* **2001**, *241*, 297−301.
(26) Kamiya, Y.; Mizoguchi, K.; Terada, K.; Fujiwara, Y.; Wang, J.-S. *Macromolecules* **1998**, *31*, 472−478.
(27) Wang, J.-S.; Kamiya, Y.; Naito, Y. *J. Polym. Sci. Part B: Polym. Phys.* **1998**, *36*, 1695−1702.
(28) Gustafsson, Ö.; Bucheli, T. D.; Kukulska, Z.; Andersson, M.; Largeau, C.; Rouzaud, J.-N.; Reddy, C. M.; Eglinton, T. I. *Global Biogeochem. Cycles* **2001**, *15*, 881−890.
(29) Palotás, A. B.; Rainey, L. C.; Feldermann, C. J.; Sarofim, A. F.; Van der Sande, J. B. *Microsc. Res. Technol.* **1996**, *33*, 266.
(30) Harris, P. J. F.; Tsang, S. C. *Philos. Mag. A* **1997**, *76*, 667.
(31) Shibuya, M.; Kato, M.; Ozawa, M.; Fang, P. H.; Osawa, E. *Fullerene Sci. Technol.* **1999**, *7*, 181−193.
(32) Xia, G.; Ball, W. P *Environ. Sci. Technol.* **1999**, *33*, 262−269.
(33) Boehm, H. P. *Carbon* **1994**, *32*, 759−769.
(34) Miyawaki, J.; Kanda, T.; Kaneko, K. *Langmuir* **2001**, *17*, 664−669.
(35) Manes, M. In *Encyclopedia of Environmental Analysis and Remediation*; Meyers, R. A., Ed.; John Wiley: New York, 1998; pp 26−68.
(36) Buiel, E. R.; George, A. E.; Dahn, J. R. *Carbon* **1999**, *37*, 1399−1407.
(37) Glaser B.; Haumaier, L.; Guggenberger G.; Zech, W. *Org. Geochem.* **1998**, *29* (4), 811−819.

(38) Mao, J. D.; Hu, W.-G.; Schmidt-Rohr, K.; Davis, G.; Ghabbour, E. A.; Xing, B. *Soil Sci. Soc. Am. J.* **2000**, *64*, 873−884.
(39) Xing, B.; Mao, J.; Hu, W.-G.; Schmidt-Rohr, K.; Davies, G.; Ghabbour, E. A. In *Understanding Humic Substances: Advanced Methods, Properties and Applications*; Davies, G., Ghabbour, E. A., Eds.; The Royal Society of Chemistry: Cambridge, 1999; pp 49−61.
(40) Neimark, A. V.; Ravikovitch, P. I.; Grün, M.; Schüth, F.; Unger, K. K. *J. Colloid Interface Sci*. **1998**, *207*, 159−169.
(41) Ravikovitch, P. I.; Vishnyakov, A.; Russo, R.; Neimark, A. V. *Langmuir* **2000**, *16*, 2311−2320.
(42) Vishnyakov, A.; Ravikovitch, P. I.; Neimark, A. V. *Langmuir* **1999**, *15*, 8736−8742.
(43) U.S. Environmental Protection Agency. *Handbook of RCRA Ground Water Monitoring Constituents: Chemical and Physical Properties*; 40 CFR Part 264, Appendix IX; National Technical Information Service: Springfield, VA, 1992.
(44) Liu, C.; Evett, J. B. *Soil Properties. Testing, Measurements, and Evaluation*, 2nd ed.; Prentice Hall Career & Technology: Englewood Cliffs, NJ, 1990.
(45) Lyon, W. G.; Rhodes, D. A. EPA/600/2-91/033. Robert S. Kerr Environmental Research Laboratory, Office of Research and Development, U.S. EPA: 1991.
(46) Neimark, A. V. In *Proceedings of the 6th Conference on Theoretical Aspects of Adsorption*, Nauka, Moscow, 1985; p 167 (in Russian).
(47) Neimark, A. V. *Dokl. Akad. Nauk SSSR* **1985**, *281*, 383−388.
(48) Neimark, A. V.; Ravikovitch, P. I.; Vishnyakov, A. *Phys. Rev. E* **2000**, *62*, R1493−R1496.
(49) Brunauer, S.; Emmett, P. H.; Teller, E. *J. Am. Chem. Soc.* **1938**, *60*, 309.
(50) Ross, M. M.; Risby, T. H.; Steele, W. A.; Lestz, S. S.; Yasbin, R. E. *Colloids Surf.* **1982**, *5*, 17−31.
(51) Jonker, M. T. O.; Koelmans, A. A. *Environ. Sci. Technol.* **2002**, *36*, 4107−4113.
(52) Olivier, J. P. *Carbon* **1998**, *36*, 1469−1472.

Received for review March 25, 2002. Revised manuscript received November 1, 2002. Accepted November 6, 2002.

ES020660Z